# Condensation of Coherent Structures in Turbulent Flows

Kai Leong Chong (庄启亮), Shi-Di Huang (黄仕迪), Matthias Kaczorowski, and Ke-Qing Xia (夏克青)
*Department of Physics, The Chinese University of Hong Kong, Shatin, Hong Kong, China*
(Received 13 September 2015; published 30 December 2015)

Coherent structures are ubiquitous in turbulent flows and play a key role in transport. The most important coherent structures in thermal turbulence are plumes. Despite being the primary heat carriers, the potential of manipulating thermal plumes to transport more heat has been overlooked so far. Unlike some other forms of energy transport, such as electromagnetic or sound waves, heat flow in fluids is generally difficult to manipulate, as it is associated with the random motion of molecules and atoms. Here we report how a simple geometrical confinement can lead to the condensation of elementary plumes. The result is the formation of highly coherent system-sized plumes and the emergence of a new regime of convective thermal turbulence characterized by universal temperature profiles and significantly enhanced heat transfer. It is also found that the universality of the temperature profiles and heat transport originate from the geometrical properties of the coherent structures, i.e., the thermal plumes. Therefore, in contrast to the classical regime, boundary layers in this plume-controlled regime are being controlled, rather than controlling.

DOI: 10.1103/PhysRevLett.115.264503 PACS numbers: 47.27.De, 44.25.+f, 47.27.T-

The existence of coherent structures is one of the defining features that distinguishes turbulent flows from purely random ones. As coherent structures are more efficient for large-scale transport of mass, momentum, and heat, they play crucial roles in turbulent transport [1–3]. Therefore, the ability of manipulating these structures to enhance transport would be highly desirable. One example is convective heat transfer, which is a fundamental process involved in many turbulent flows. Convective heat transfer in the classical regime is limited by thermal diffusion in the boundary layers (BLs). Thus, efforts to increase heat transfer efficiency are typically focused on boundary modifications or increasing shear at the BLs by making flows more turbulent [4]. These traditional methods have become standard solutions for passive heat transfer enhancements, which are highly preferred and sometimes are even essential requirements in many engineering and industrial applications, such as convective heat transfer in nuclear reactors. On the other hand, thermal plumes, being the most important coherent structures in turbulent convection, are known as elementary heat carriers that are responsible for coherent heat transfer in the system [5,6]. A natural question then is: Can plumes be manipulated to contain more heat? In this Letter, using a classical model, the turbulent Rayleigh-Bénard (RB) convection, we show that one way to manipulate thermal plumes is through a simple geometrical confinement to the system, which results in plume condensation, i.e., the formation of system-sized giant plumes. This leads to the emergence of a new regime of significantly enhanced heat transfer, in which the efficiency is controlled by the properties of thermal plumes rather than BLs.

The RB system, a fluid layer heated from below and cooled from above, has become a paradigm for the study of convective thermal turbulence [7–12]. The flow dynamics of the system are characterized by the Rayleigh number $\mathrm{Ra} = \alpha g \Delta T H^3/\nu\kappa$, the Prandtl number $\mathrm{Pr} = \nu/\kappa$, and the aspect ratio $\Gamma$, with $\alpha$, $\nu$, and $\kappa$ being the thermal expansion coefficient, kinematic viscosity, and thermal diffusivity of the convecting fluid, $g$ the gravitational acceleration, and $\Delta T$ the temperature difference across the convection cell. The efficiency of heat transport and turbulent intensity in the system are expressed in terms of the nondimensional heat flux Nusselt number Nu and the Reynolds number Re. In the present study a direct numerical simulation method was employed [13–15] and the details are provided in the Supplemental Material [16]. Our numerical experiment was conducted in a fluid bounded in a rectangular box of height $H$, length $L$, and width $W$ and spanned the parameter ranges of $1\times10^7 \le \mathrm{Ra} \le 1\times10^{10}$ and of $1/64 \le \Gamma(=W/H) \le 1$, all at fixed $\mathrm{Pr} = 4.38$. It has been generally accepted that in turbulent convection $\Gamma$ has only a minimal effect on Nu, as it cannot significantly influence the thermal BL thickness [9,17–21]. However, in Fig. 1(a) we show that the response of the global convective heat transfer to the geometric confinement is remarkably strong and highly nontrivial: As $\Gamma$ decreases, Nu increases significantly above its $\Gamma = 1$ value, and for each Ra there exists a maximum Nu at a well-defined aspect ratio, $\Gamma_{\mathrm{opt}}$ (the optimal aspect ratio), below which Nu drops sharply.

By plotting $Nu/Nu_{\mathrm{max}}$ vs $\Gamma/\Gamma_{\mathrm{opt}}$ [Fig. 1(b)], all data fall on top of each other, once $\Gamma$ is smaller than a Ra-dependent aspect ratio (denoted as onset aspect ratio $\Gamma_c$). This signals that turbulent flow may have entered a new regime with universal heat transport properties when $\Gamma < \Gamma_c$. This universality is made clearer in Fig. 1(c) where temperature profiles for different Ra and $\Gamma$, but all having $\Gamma = \Gamma_{\mathrm{opt}}$, collapse excellently onto a single curve. In contrast, profiles at fixed $\Gamma$ but with different values of Ra differ drastically

 

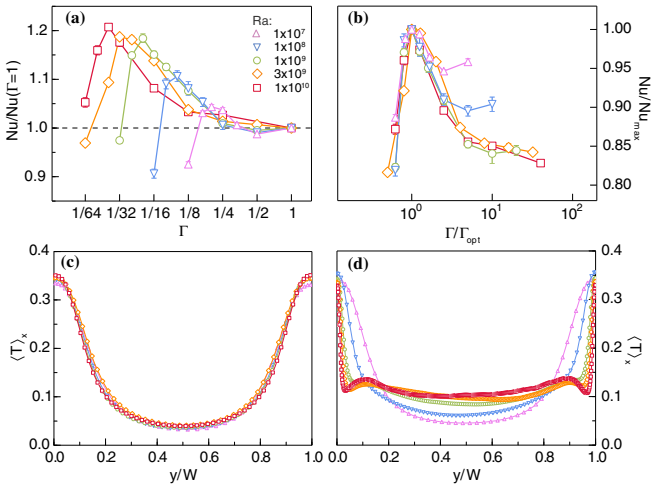


FIG. 1 (color online). (a) The normalized global Nu as a function of $\Gamma$ over 3 decades of Ra. The lines are drawn to guide the eye. (b) $\mathrm{Nu}/\mathrm{Nu}_{\mathrm{max}}$ is plotted against $\Gamma/\Gamma_{\mathrm{opt}}$. Here, $\Gamma_{\mathrm{opt}}$ is the optimal aspect ratio at which a maximum value $\mathrm{Nu}_{\mathrm{max}}$ is achieved. (c) Mean temperature profiles along the direction $y$ (the smallest dimension) in cells with $\Gamma = \Gamma_{\mathrm{opt}}$ for different values of Ra. The profiles are obtained at a distance $z = \delta_{\mathrm{th}}$ above the bottom plate, where $\delta_{\mathrm{th}}$ is the thickness of the thermal boundary layer. (d) Mean temperature profiles for different values of Ra similar to those in (c), but now all have fixed $\Gamma = 1/4$. Temperature is averaged over time and the cell length $L$. All the legends are the same as in (a).

from each other [Fig. 1(d)]. This suggests that, besides $\Gamma_c$, $\Gamma_{\mathrm{opt}}$ is also a characteristic quantity of the system. What then are the physical origins for the existence of the onset and optimal aspect ratios?

As the thermal BL thickness is still much smaller than the system width at $\Gamma_c$, it is unlikely to be perturbed directly by confinement. Instead, such confinement should strongly influence the flow structures. This led us to examine how plumes respond to confinement, as they are the most important coherent flow structures in thermal convection. As shown in Figs. 2(a) and 2(b), plumes exhibit cellular structures for the unconfined cases ($\Gamma = 1$), consistent with previous findings [22,23]. We first examine the $\mathrm{Ra} = 1 \times 10^8$ case [Fig. 2(a)], which shows that at $\Gamma = 1/4$ the separation of the plumes becomes comparable to the width of the cell. Thus, further confinement to $\Gamma = 1/8$ yields a transition to a different plume morphology; i.e., the two-dimensional (2D) cellular plumes now become 1D lines roughly perpendicular to the front and back walls of the cell (or parallel to the $y$ direction). In contrast, for $\mathrm{Ra} = 1 \times 10^{10}$ [Fig. 2(b)], even at $\Gamma = 1/8$ the cellular structure is largely unperturbed, and only until a more severe confinement at $\Gamma = 1/16$ is reached does the plume morphology change to 1D structure.

These changes in plume morphology coincide with the first transition in Nu-$\Gamma$ behavior shown in Fig. 1, indicating

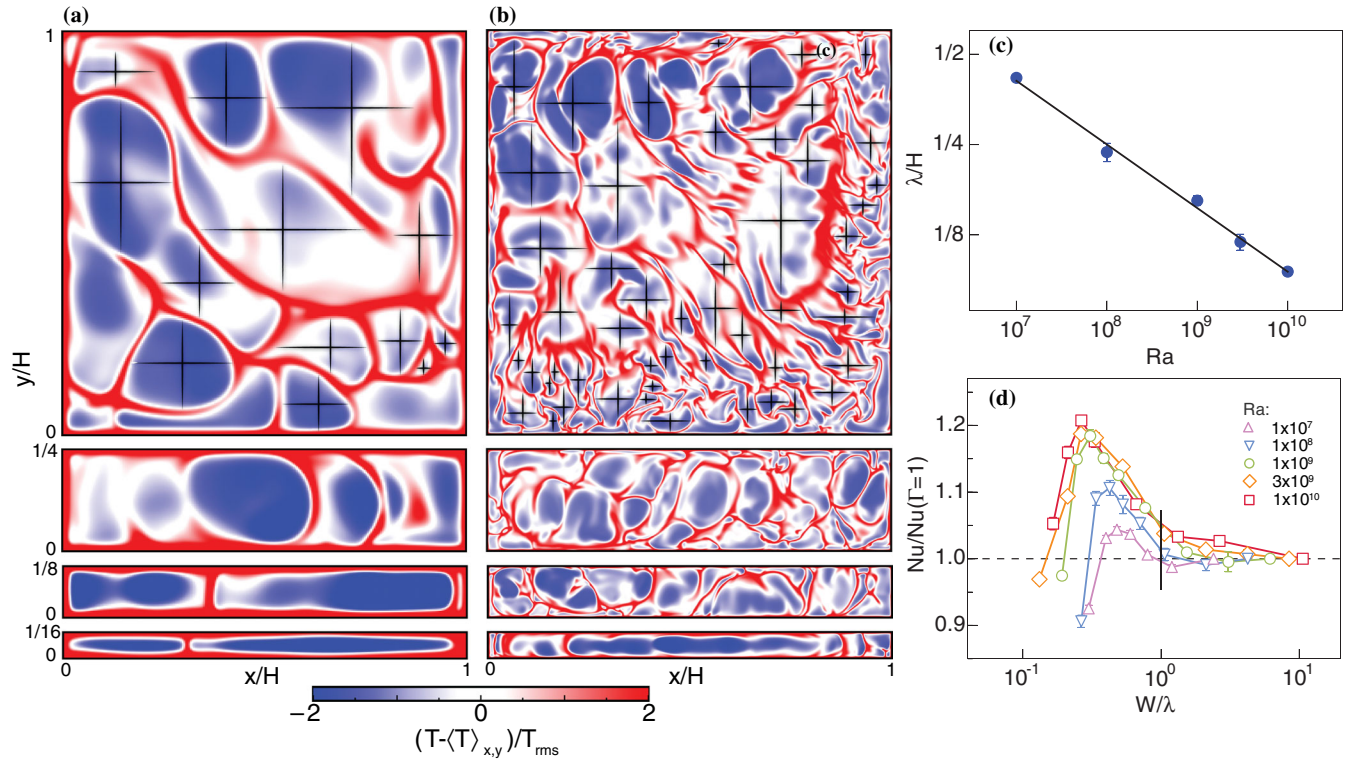


FIG. 2 (color online). (a) and (b) Horizontal cuts of instantaneous standardized temperature field $(T - \langle T \rangle_{x,y})/T_{\mathrm{rms}}$ taken at the edge of the thermal boundary layer near the bottom plate. (The crosses are used to determine the plume spacing, see Methods in Supplemental Material [16] for details.) Left panel: $\mathrm{Ra} = 1 \times 10^8$. Right panel: $\mathrm{Ra} = 1 \times 10^{10}$. In both (a) and (b), the aspect ratios are, from top to bottom, $\Gamma = 1, 1/4, 1/8$, and $1/16$. The same results are obtained for the top plate because of the top-bottom symmetry of the system. (c) Normalized mean plume spacing $\lambda/H$ vs Ra; the solid line represents the best power law fit $\lambda/H = 12.42\mathrm{Ra}^{-0.21\pm0.01}$ to the data points. (d) $\mathrm{Nu}/\mathrm{Nu}(\Gamma = 1)$ versus $W/\lambda$.

that the typical size of cellular structure plays a crucial role in determining $\Gamma_c$, which then defines a characteristic length, the mean plume spacing $\lambda$ that can be used to quantify $\Gamma_c$ [see Methods in Supplemental Material [16] for details on how $\lambda$ is determined and Fig. 2(c) for the obtained results]. Indeed, when $\mathrm{Nu}/\mathrm{Nu}(\Gamma = 1)$ is replotted vs the normalized $W/\lambda$ [note that $W/\lambda = \Gamma/(\lambda/H)$], all curves begin a significant rise with roughly the same slope when $W/\lambda < 1$ [Fig. 2(d)]. This clearly demonstrates that it is the plume morphology, characterized by $\lambda$, that determines the onset $\Gamma_c$ (i.e., $W_c/\lambda = 1$).

We examine next the horizontal slices of instantaneous temperature field at $\Gamma = \Gamma_{\mathrm{opt}}$ [Figs. 3(a) and 3(b)]. A striking feature seen is that a large area of the top and bottom plates is now covered by a few large and highly coherent thermal plumes; i.e., the hot bottom plate is covered by cold plumes and the cold top plate by hot plumes. This is found to be true for all values of Ra studied. The temperature field at different heights suggests that these system-sized (or "giant") and highly coherent plumes are formed as hot (cold) "elementary plumes" travel upwards (downwards) and merge with likewise plumes. This merging of plumes as they traverse the height of the cell is demonstrated by the time sequence of temperature fields taken at different heights [Fig. 3(c)]. These images show that the hot plumes are first emitted from the gaps between giant cold plumes and/or between the cold plumes and the sidewall at the bottom hot boundary layer; they then merge into larger plumes as they travel upwards and finally condense into a giant plume at the top cold boundary layer. This process of plume condensation is further illustrated by the movies in the Supplemental Material [16]. The present study thus reveals how elementary plumes condense into giant plumes by geometrical confinement. Confinement-induced Nu enhancement was observed in a previous study and was attributed to the increased plume coherency [24]. The physical mechanism of plume condensation identified here implies that the optimal aspect ratio $\Gamma_{\mathrm{opt}}$ (or, equivalently the optimal cell width $W_{\mathrm{opt}}$) observed in the present work corresponds to the maximum size that plumes can condense into. Thus, the origin of the universality and the maximum heat transfer should be related to the geometrical properties of plumes, as shown in Figs. 3(d) and 3(e). It is seen clearly that the normalized plume width $d/W$ and length $\ell/L$ at $\delta_{th}$ reach maximum values at $\Gamma_{\mathrm{opt}}$ and exhibit universal properties when plotted

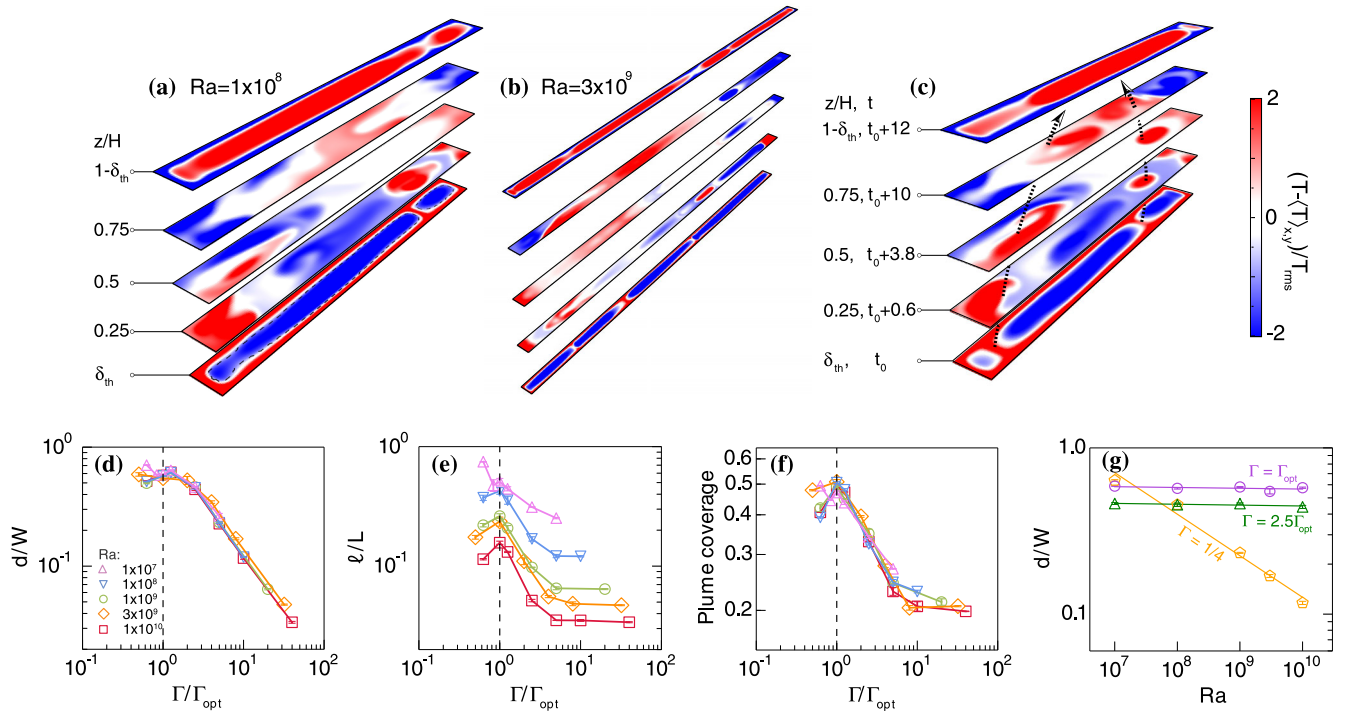


FIG. 3 (color online). Horizontal slices of the instantaneous standardized temperature field $(T - \langle T\rangle_{x,y})/T_{\mathrm{rms}}$ at the optimal aspect ratio $\Gamma_{\mathrm{opt}}$, for $\mathrm{Ra} = 1 \times 10^8$ (a) and $3 \times 10^9$ (b). The vertical heights of the horizontal cut are as indicated, where $\delta_{\mathrm{th}}$ is the thermal boundary layer thickness. Note that the instantaneous temperature fields in (a) are taken at the same time, and so are those in (b). (c) Time sequence of standardized temperature fields taken at different heights for $\mathrm{Ra} = 1 \times 10^8$. The black dashed arrows are drawn to indicate how "elementary" hot plumes evolve into a "giant" hot plume as they traverse the height of the cell from certain time $t_0$ to $t_0 + 12$ (in free-fall time unit). (d) Normalized plume width $d/W$ at $\delta_{th}$, defined along the cell width $W$, vs normalized aspect ratio $\Gamma/\Gamma_{\mathrm{opt}}$. (e) Normalized plume length $\ell/L$ at $\delta_{th}$, defined along the cell length $L$, vs $\Gamma/\Gamma_{\mathrm{opt}}$. (f) Percentage of plume coverage at $\delta_{\mathrm{th}}$ vs $\Gamma/\Gamma_{\mathrm{opt}}$. (g) Normalized plume width at $\delta_{th}$ vs Ra for $\Gamma = \Gamma_{\mathrm{opt}}$, $\Gamma = 2.5\Gamma_{\mathrm{opt}}$ and at fixed $\Gamma = 1/4$ (unconfined cases), respectively.

against $\Gamma/\Gamma_{\rm opt}$; for $d/W$ a nearly complete collapse, and for $\ell/L$ collapse can be achieved when a proper vertical shift is made [25]. The quantity that can best characterize the universal property of heat transfer is the plume coverage, defined as the fractional area occupied by hot (cold) plumes at the top (bottom) plate. It, too, exhibits a universal behavior [Fig. 3(f)]. In contrast to the unconfined cases, in which the coverage by elementary plumes is ~20%, at the optimal aspect ratio, coverage by the giant plumes reaches to ~50%; the remaining area is left for the emission of plumes (of the opposite sense) from the plate and for the region taken up by the viscous BL at the sidewalls. This also explains why $d/W$ has a maximum value of less than one (~0.6), indicating that a single plume essentially fills up the "available" width of the cell [see also Figs. 3(a) and 3(b)]. Thus, as $W$ (or $\Gamma$) reduces and plumes grow, a maximum plume width $d_{\rm max}$ is eventually reached that also fixes the optimal aspect ratio $\Gamma_{\rm opt}$; i.e., $d_{\rm max}$ and $\Gamma_{\rm opt}$ are essentially the same quantity [Fig. 3(g)].

It is now clear that the universality of the global heat transfer in the new regime is a result of the universal properties of the plume morphology and coverage at the BL, and a maximum heat transfer efficiency is achieved when plume coverage reaches maximum. In this context, we call the new regime the plume-controlled regime. We note that the universal properties are not limited at $\Gamma/\Gamma_{\rm opt} = 1$; as long as the ratio $\Gamma/\Gamma_{\rm opt}$ has the same value and is within the plume-controlled regime, plumes will exhibit universal properties [Fig. 3(g)]. In contrast, $d/W$ shows strong Ra dependence at fixed $\Gamma$. The same is also found to be true for temperature profiles (see Supplemental Material Fig. 1 [16]).

We have shown how elementary thermal plumes condense into highly coherent ones by geometrical confinement, which in turn leads to a significantly increased global heat transfer efficiency. The universal temperature profiles at the BL [Fig. 1(c)] can now be understood from the universality of the plume width; i.e., the width of their flat bottom is just about 0.6, which is the same as the plume width at $\Gamma_{\rm opt}$. In addition, owing to their increased size and coherency, the cold (hot) plumes at the hot bottom (cold top) plate are colder (hotter) than they typically are in the unconfined cases, which results in a thinner and more uniform BL. In fact the BL at the optimal aspect ratio $\Gamma_{\rm opt}$ is overall the thinnest and flattest and also has a universal shape of a flat bottom of width ~0.6, indicating that it too originates from the universal plume width (see Supplemental Material Fig. 2 [16]). This shows that the BLs are now being controlled, rather than controlling, which distinguishes the new regime from the classical one. The transition from the classical boundary-layer controlled regime to the this plume-controlled one is brought about by the change in plume morphology in the 2D plane near the boundary layer when the cell width becomes comparable to the the mean plume spacing, which gives rise to an onset aspect ratio $\Gamma_c$. As the coherent plumes grow in their size

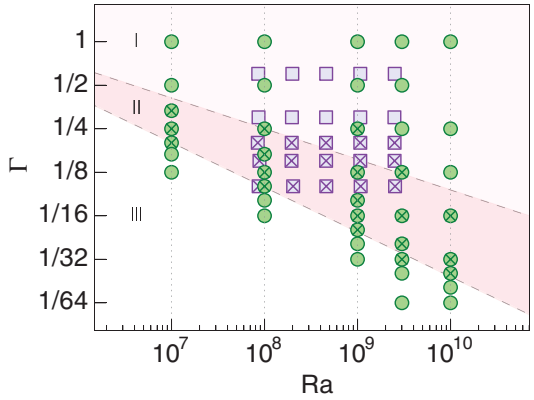


FIG. 4 (color online). Phase diagram showing the various regimes of heat transport: Regime I is the classical boundary layer controlled regime. Regime II is the plume controlled regime, which is defined by the onset aspect ratio $\Gamma = 12.42{\rm Ra}^{-0.21}$ (upper dashed line) related to mean plume spacing; and by $\Gamma = 29.37{\rm Ra}^{-0.31}$ (lower dashed line), which is a fit to the observed optimal aspect ratio $\Gamma_{\rm opt}$. The circles represent simulations from the present study and squares from a previous experiment [24]. The symbols marked with a cross indicate that the obtained Nu behavior for the corresponding datum is in Regime II.

with increasing confinement, their width eventually becomes comparable to the cell width, which then defines an optimal aspect ratio $\Gamma_{\rm opt}$ for maximum heat transfer. This leads to the emergence of system-sized giant coherent plumes at $\Gamma_{\rm opt}$ and maximum plume coverage at the conducting plates. To give an overall picture of the different heat transfer regimes we present a phase diagram in Fig. 4, which includes data points from the present numerical study and a previous experiment [24]. In the figure the new plume-controlled regime is labeled as Regime II, the classical boundary layer-controlled regime is labeled as Regime I, and the regime when $\Gamma$ becomes smaller than $\Gamma_{\rm opt}$ and the flow is dominated by viscous boundary layers from the sidewall is labeled as Regime III. We note that the width of Regime II grows with increasing Ra, suggesting that there is a wider parameter range for the plume controlled regime and optimal heat transport at higher values of Ra. The figure symbols marked with a cross indicate that Regime II behavior is observed for the corresponding data based the obtained Nu, which shows a very good agreement with the demarcation of Regime II as defined by the two dashed lines. Finally we remark that the increased heat transfer efficiency is achieved despite the increased drag from the sidewalls that results in a reduction of the Reynolds number (see Supplemental Material Fig. 3 [16]). This decoupling between heat transport and momentum or mass transport is another characteristic of the plume-controlled regime.

In closing, we have shown how coherent structures in turbulent flows can be manipulated through a simple geometrical confinement, using thermal plumes as an

example. This manipulation leads to the phenomenon of coherent structure condensation. Furthermore, our study has shown a direct link between global quantities and the properties of elementary carriers (of heat) in turbulent flows. It provides an example of how coherent structure manipulation can control the global transport properties of the turbulent flow. In the present case it is heat transfer, but in principle it can be momentum, angular momentum, or kinetic energy transfers, such as in pipe flow, Taylor-Couette flow, etc. Moreover, if the condensation of coherent structures can be realized in other turbulence systems, it will have a far reaching effect in turbulent transport.

This work was supported by the Hong Kong Research Grants Council under the Projects No. CUHK 403712 and No. 404513, and through a Hong Kong PhD Fellowship. We are also grateful for the support of computational resources by the Leibnitz-Rechenzentrum Munich under the Project No. pr47vi and the High Performance Cluster Computing Centre, Hong Kong Baptist University.

[1] A. K. M. Hussain, J. Fluid Mech. **173**, 303 (1986).
[2] L. Sirovich, Q. Appl. Math. **45**, 561 (1987).
[3] P. Holmes, J. L. Lumley, and G. Berkooz, *Turbulence, Coherent Structures, Dynamical Systems and Symmtry* (Cambridge University Press, Cambridge, 1998).
[4] T. L. Bergman, F. P. Incropera, and A. S. Lavine, *Fundamentals of Heat and Mass Transfer* (John Wiley & Sons, New York, 2011).
[5] X.-D. Shang, X.-L. Qiu, P. Tong, and K.-Q. Xia, Phys. Rev. Lett. **90**, 074501 (2003).
[6] E. S. C. Ching, H. Guo, X.-D. Shang, P. Tong, and K.-Q. Xia, Phys. Rev. Lett. **93**, 124501 (2004).
[7] E. D. Siggia, Annu. Rev. Fluid Mech. **26**, 137 (1994).
[8] L. P. Kadanoff, Phys. Today **54**, No.08, 34 (2001).
[9] G. Ahlers, S. Grossmann, and D. Lohse, Rev. Mod. Phys. **81**, 503 (2009).
[10] D. Lohse and K.-Q. Xia, Annu. Rev. Fluid Mech. **42**, 335 (2010).
[11] F. Chillà and J. Schumacher, Eur. Phys. J. E **35**, 58 (2012).
[12] K.-Q. Xia, Theor. Appl. Mech. Lett. **3**, 052001 (2013).
[13] M. Kaczorowski, A. Shishkin, O. Shishkina, and C. Wagner, New Results Numeric. Experi. Fluid Mech. VI **96**, 381 (2008).
[14] O. Shishkina, R. J. A. M. Stevens, S. Grossmann, and D. Lohse, New J. Phys. **12**, 075022 (2010).
[15] M. Kaczorowski and K.-Q. Xia, J. Fluid Mech. **722**, 596 (2013).
[16] See Supplemental Material at http://link.aps.org/supplemental/10.1103/PhysRevLett.115.264503 for numerical details, plume extraction methods, supplemental figures, and movies.
[17] A. Nikolaenko, E. Brown, D. Funfschilling, and G. Ahlers, J. Fluid Mech. **523**, 251 (2005).
[18] C. Sun, L.-Y. Ren, H. Song, and K.-Q. Xia, J. Fluid Mech. **542**, 165 (2005).
[19] J. Bailon-Cuba, M. S. Emran, and J. Schumacher, J. Fluid Mech. **655**, 152 (2010).
[20] E. P. van der Poel, R. J. A. M. Stevens, and D. Lohse, Phys. Rev. E **84**, 045303 (2011).
[21] Q. Zhou, B.-F. Liu, C.-M. Li, and B.-C. Zhong, J. Fluid Mech. **710**, 260 (2012).
[22] B. A. Puthenveettil and J. H. Arakeri, J. Fluid Mech. **542**, 217 (2005).
[23] Q. Zhou, C. Sun, and K.-Q. Xia, Phys. Rev. Lett. **98**, 074501 (2007).
[24] S.-D. Huang, M. Kaczorowski, R. Ni, and K.-Q. Xia, Phys. Rev. Lett. **111**, 104501 (2013).
[25] The datum at the smallest $\Gamma$ for $\mathrm{Ra} = 1 \times 10^7$ appears to exhibit a different trend than the other points. We note that for this lowest value of Ra and $\Gamma$ the effect of the viscous drag from the sidewalls is strongest and the flow is therefore less turbulent.